

Many-body effects in tracer particle diffusion with applications for single-protein dynamics on DNA

Sebastian Ahlberg

Integrated Science Lab, Department of Physics, Umeå University, SE-901 87 Umeå, Sweden

Tobias Ambjörnsson

*Department of Astronomy and Theoretical Physics,
Lund University, Sölvegatan 14A, SE-223 62 Lund, Sweden*

Ludvig Lizana

*Integrated Science Lab, Department of Physics, Umeå University, SE-901 87 Umeå, Sweden **

(Dated: August 9, 2021)

30% of the DNA in *E. coli* bacteria is covered by proteins. Such high degree of crowding affect the dynamics of generic biological processes (e.g. gene regulation, DNA repair, protein diffusion etc.) in ways that are not yet fully understood. In this paper, we theoretically address the diffusion constant of a tracer particle in a one dimensional system surrounded by impenetrable crowder particles. While the tracer particle always stays on the lattice, crowder particles may unbind to a surrounding bulk and rebind at another or the same location. In this scenario we determine how the long time diffusion constant \mathcal{D} (after many unbinding events) depends on (i) the unbinding rate of crowder particles k_{off} , and (ii) crowder particle line density ρ , from simulations (Gillespie algorithm) and analytical calculations. For small k_{off} , we find $\mathcal{D} \sim k_{\text{off}}/\rho^2$ when crowder particles are immobile on the line, and $\mathcal{D} \sim \sqrt{Dk_{\text{off}}}/\rho$ when they are diffusing; D is the free particle diffusion constant. For large k_{off} , we find agreement with mean-field results which do not depend on k_{off} . From literature values of k_{off} and D , we show that the small k_{off} -limit is relevant for *in vivo* protein diffusion on a crowded DNA. Our results applies to single-molecule tracking experiments.

I. INTRODUCTION

Few doubt that molecular crowding has severe consequences for dynamical processes [1]. Interesting examples are living cells where macromolecular concentrations are large. Take the *E. coli* bacterium as an example. There, the concentration of proteins and RNA is about 300–400 mg/ml [2] which is 30–40 times larger than common test tube conditions [3]. There is overwhelming evidence that this level of crowding influences important biological processes such as gene regulation [4], enzymatic activity [5], protein folding [6, 7], and diffusion of macromolecules [8, 9]. In order to get a complete picture of the *in vivo* dynamics we must increase our understanding of the role of crowding, and recent experimental developments provide the means to do it.

In recent years, researchers have beat the diffraction limit and turned optical microscopy into ‘nanoscopy’. Today’s microscopy methods (e.g. STED, STORM and FIONA) [10] does not only allow us to image nanometer-sized biological structures, but recent improvements [11, 12] also permit tracking fluorescently labelled proteins at the biologically relevant millisecond-scale. This is anticipated to shed new light on biological processes, as well as increase our understanding of particle transport in engineered nano-fluidic systems [13, 14]. In order to properly interpret those type of experiments *in vivo*, we

need new theoretical and computational models in terms of physical properties of the intracellular space, the cytoplasm.

The cytoplasm is cramped with macromolecules and we are interested how this influences diffusion-controlled processes, a key component in many cellular functions (e.g. gene regulation). While our results are new, aspects of this problem has been studied theoretically before. For example, [15–18] investigate diffusion in the three dimensional cytoplasm and in gels, whereas [19–22] focus on the sub-diffusive motion seen in single-molecule experiments. Crowding is also important for DNA search processes where a searcher combines one and three dimensional diffusion to quickly find its target, so called facilitated diffusion. Facilitated diffusion under crowding is addressed in [4, 23] which resemble this paper but we ask different questions: we calculate the diffusion constant of a tracer particle in terms of key properties of surrounding crowder particles rather than focusing on mean target finding times.

Much inspiration to this work comes from DNA binding proteins. Of particular interest is repair proteins (MutS and homologs) whose residence time on the DNA can be very long (~ 10 min [24]). We are also inspired by transcription factors, the family of gene regulatory proteins. The yeast regulatory proteins LexA and Gal4 can stay bound to their regulatory sites for several minutes *in vitro* (LexA ~ 5 min and Gal4 > 30 min) [25], but surprisingly, this number can be reduced up to 1000 times *in vivo*. Both classes of proteins have the ability to diffuse along the DNA, unbind to the three dimensional intra-

*Electronic address: ludvig.lizana@physics.umu.se

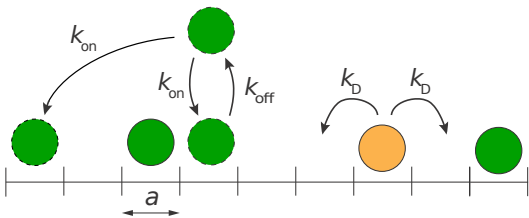


FIG. 1: Schematic illustration of our model. All particles are diffusing with rate k_D on a one dimensional lattice with lattice spacing a . The crowder particles (green) may also unbind and rebound to a random, or the same, lattice site with rates k_{off} and k_{on} , respectively. The tagged particle (orange) cannot leave the line ($k_{on} = k_{off} = 0$).

cellular space, diffuse in space, and rebound to the DNA. We are interested in how the dynamics of those proteins change under crowding.

In order to better understand the role of crowding, we introduce a theoretical model where particles diffuse on a one dimensional lattice where two particles cannot occupy the same site (Fig. 1). They diffuse with rate k_D (same for all particles) and may unbind and rebound to the lattice with rates k_{off} and k_{on} , respectively. These rates are tuned so that the average particle line density is constant at 10-20% which is not too far from *in vivo* conditions (30% of the DNA in *E. coli* is covered by proteins). The unbinding rate for the tracer particle is set to zero similar to the long-lived protein-DNA complexes described above. Now we ask:

What is the long time diffusion constant of a tracer particle in such a crowded quasi one dimensional system?

We answer this question numerically using stochastic simulations (Gillespie algorithm), corroborated with analytical results. The main results are Figs. 4–6 where we show how the diffusion constant changes as a function of our main parameter k_{off} . Those results are applicable to single molecule tracking experiments [26].

The unbinding rate k_{off} interpolates between two well studied limits. (i) When k_{off} is large (compared to k_D), the tracer’s mobility is only weakly lowered and diffuses close to as if it was free. (ii) When $k_{off} \rightarrow 0$, the particles diffuse with unchanged order in a single file. Single-file diffusion is well studied [27–33] where the most famous result is that the mean squared displacement of a tracer particle is proportional to \sqrt{t} rather t (t is time) which signatures non-markovian dynamics.

This paper is organised as follows. In Sec. II, we outline briefly the details of our model. Before showing the results in Sec. IV, we provide analytical estimates of the diffusion constant in Sec. III, based on a theoretical calculation found in Appendix A. In Sec. III we also briefly review the dynamics of the model at short, intermediate and long times. We close by a few concluding remarks in Sec. V.

II. THE MODEL

Our model has been used and explained elsewhere [34], but for completeness we summarise it briefly below. Consider a one dimensional lattice on which crowder particles (assumed identical) and the tracer particle diffuse (Fig. 1). The crowder particles can diffuse, unbind and rebound to the lattice. Rebinding occurs in two ways. Either to a random unoccupied lattice site (chosen with uniform probability), or to the exact same location. Both rebinding modes has been used to model transcription factor dynamics on DNA [35, 36], and we will therefore consider both. The lattice constant is denoted a , and the diffusion rate k_D is assumed equal in both directions and for all particles. Double occupancy is forbidden and a particle cannot overtake a flanking neighbor (single-file condition). Binding and unbinding dynamics of crowders are characterised by the rates k_{on} and k_{off} , which are chosen such that the particle line density is in equilibrium with the bulk, thereby keeping the average filling fraction is constant. In our simulations we keep it at 10–20%. We implemented the model using the Gillespie algorithm. See Appendix C for details.

III. ANALYTICAL ESTIMATES FOR THE LONG TIME DIFFUSION CONSTANT

Here we provide analytical estimates to corroborate and better understand the numerical results in the next section. We are mainly interested in the long time diffusion \mathcal{D} constant for the tracer particle, defined as

$$\langle x^2(t) \rangle \simeq 2\mathcal{D}t \quad (1)$$

where $\langle x^2(t) \rangle$ is the ensemble averaged mean squared displacement (MSD), and t is time. Notably, \mathcal{D} is in general not equal to the bare, or free particle, diffusion constant

$$D = a^2 k_D. \quad (2)$$

It is a non-trivial function of k_{off} and ρ . To better understand what we mean by long time, we describe in subsection III D the dynamics leading up to Eq. (1). But first we summarise our main analytical findings from Appendix A which we in Sec. IV compare to simulations.

A. Long time, small k_{off} behaviour

To simplify matters, we start by assuming that the crowder particles sit equidistantly on the line with density ρ , unable to diffuse ($k_D = 0$), and rebound to the site from which they unbound. In this situation, the tracer moves back and fourth between its flanking neighbours and can only move past them if one of them unbinds. The average time until this happens is proportional to $1/k_{off}$. In point of view of the tracer this process is a random walk on an effective, or coarse grained, lattice

with spacing and jump rate proportional to $1/\rho$ and k_{off} , respectively. From this we expect that $\mathcal{D} \sim k_{\text{off}}/\rho^2$, and a more elaborate calculation shows that

$$\mathcal{D} \simeq \frac{3(1-a\rho)k_{\text{off}}}{4\rho^2}. \quad (3)$$

When crowder particles rebind to a random location rather than to the same site, the distance between two neighbouring particles fluctuate even though the average density is fixed. This leads to a larger effective lattice spacing, and a larger \mathcal{D} compared to Eq. (3):

$$\mathcal{D} \simeq \frac{(2-a\rho)(1-a\rho)}{4\rho^2} k_{\text{off}}. \quad (4)$$

When crowder particles also diffuse ($k_D \neq 0$) the distance between nearest-neighbours becomes difficult to define. We estimate the coarse grained lattice constant as the length the tracer particle explores during a time interval proportional to $1/k_{\text{off}}$. This leads to

$$\mathcal{D} \simeq \frac{(1-a\rho)^{3/2}}{\rho} \sqrt{\frac{Dk_{\text{off}}}{2\pi}}, \quad (5)$$

which has different k_{off} -scaling than before. Equations (3)–(5) constitute our main analytical results.

B. Long time, large k_{off} behaviour

When $k_D \gtrsim k_{\text{off}}$, crowder particles frequently unbind and rebind to the lattice and the no-passing condition is effectively violated. But, crowder particles still hinder the tracer thereby decreasing the diffusion rate. Imagine that the jump rate for a single particle to a neighbouring site on an otherwise empty lattice is k_D , or $D = a^2 k_D$. Then, when crowder particles are around, some of the jumps are canceled because the target lattice site may be occupied. In that situation the jump rate is reduced by the probability that the target lattice is unoccupied. For very large k_{off} this probability is simply $1 - a\rho$, therefore

$$\mathcal{D} \simeq D(1 - \rho a) \quad (6)$$

This mean field result has been obtained before [20, 37, 38], and as k_{off}/k_D is close to or smaller than unity, corrections to this formula becomes prominent (see Fig. 5).

C. Interpolation formula for \mathcal{D}

Based on the expressions above, we propose a simple formula for \mathcal{D} valid for all k_{off} :

$$\frac{1}{\mathcal{D}} = \frac{1}{\mathcal{D}_{\text{small } k_{\text{off}}}} + \frac{1}{\mathcal{D}_{\text{large } k_{\text{off}}}} \quad (7)$$

Here $\mathcal{D}_{\text{large } k_{\text{off}}}$ is Eq. (6) whereas $\mathcal{D}_{\text{small } k_{\text{off}}}$ is one of Eqs. (3)–(5) depending on the case under study. Equation (7) is appealingly simple and captures properly the

small and large k_{off} limits, but it should not be viewed as more than a candidate expression for \mathcal{D} . We have not made a systematic attempt to find the best form of \mathcal{D} , and leave it for future research.

D. How is the long time asymptotics [Eq. (1)] approached?

Here we clarify the meaning of short, intermediate and long times within of our model. To keep the discussion simple, we consider k_{off} , k_{on} , k_D , and ρ as constant. See also Fig. 3 which shows $\langle x^2(t) \rangle$ as a function of time, where all relevant regimes are present.

At most we have three regimes of different behaviour. These are separated by the average residence time of the crowder particles τ_{off} , and the average collision time τ_{coll} , which is the time it takes for a particle to diffuse across the average nearest neighbour distance $1/\rho$:

$$\tau_{\text{coll}} = \frac{1}{\rho^2 D}, \quad \tau_{\text{off}} = \frac{1}{k_{\text{off}}} \quad (8)$$

Let us assume that there is a clear separation between these timescales and that $\tau_{\text{coll}} \ll \tau_{\text{off}}$ and that k_D is the fastest rate in the system, $1/k_D \ll \tau_{\text{coll}}$. In the first regime, $t \ll \tau_{\text{coll}}$, the tracer diffuse as if it was free, since it has not yet collided with its nearest neighbours. This means that the tracer's MSD is $\langle x^2(t) \rangle = 2Dt$. In the second regime, $\tau_{\text{coll}} \ll t \ll \tau_{\text{off}}$, many particle collisions have taken place but particles diffuse with maintained order since they are unable to pass each other. This is the single-file diffusion regime which is characterised by Harris' law $\langle x^2(t) \rangle \propto \sqrt{Dt/\rho^2}$ [27]. Here, memory effects dominate and is the very reason to the sub diffusive behaviour. In the third regime, $t \gg \tau_{\text{off}}$, particles start unbinding from the lattice which effectively violates the no-passing condition. In this regime we expect diffusive behaviour again $\langle x^2(t) \rangle \sim t$, but with a diffusion constant different from D , denoted by \mathcal{D} [see Eq. (1)]. This is the one we wish to calculate, in particular in terms of our key parameter k_{off} . Note that the second regime can be erased completely if we lower τ_{off} such that $\tau_{\text{off}} \approx \tau_{\text{coll}}$ (or smaller). Similarly, the third regime is absent if unbinding is not allowed, i.e. $k_{\text{off}} = 0$ (or $\tau_{\text{off}} = \infty$). In most of our simulations, diffusion is the fastest process in the system which also is the likely scenario a biological cell (see Sec. V). To sum up,

$$\langle x^2(t) \rangle \simeq \begin{cases} 2Dt, & t \ll \tau_{\text{coll}} \\ (1 - \rho a)/\rho \times \sqrt{4Dt/\pi}, & \tau_{\text{coll}} \ll t \ll \tau_{\text{off}} \\ 2\mathcal{D}t, & t \gg \tau_{\text{off}} \end{cases} \quad (9)$$

IV. RESULTS

In this section we present results from stochastic simulations of the model outlined in Sec. II, together with

of our theoretical findings from Sec. III. The simulation details can be found in Appendix C. First, we show the tracer particle's MSD as a function of time, from which we extract the long time diffusion constant \mathcal{D} . Second, we investigate \mathcal{D} separately for large and small k_{off} . Finally, we compare our proposed interpolation formula Eq. (7) to the full range of k_{off} values.

A. Dynamics of the model and extraction of the long time diffusion constant

Figures 2 and 3 show the MSD of the tracer particle as a function of time, for different unbinding rates k_{off} . Symbols represent simulation results. From such plots we extract the long time diffusion constant \mathcal{D} (see Appendix B) by fitting a straight line for large times starting from $t = \tau_{\text{off}}$ (short vertical dashed lines). The results for \mathcal{D} is shown in Figs. 4–6, but first we discuss some of the features of Figs. 2 and 3.

Figure 2 shows the MSD when crowder particles do not diffuse but only unbind and rebind. They rebind either always to the same site (upper panel), or to a randomly chosen site (lower panel). The short time behaviour in both plots is independent of k_{off} and is well represented by $2Dt$ (upper dashed dark blue line). The long time behaviour is, however, strongly dependent on k_{off} , which is evident from the broad scattering of curves. The MSD is still linear in time but the diffusion constant (proportional to the extrapolated intersection with the vertical axis) depends strongly on k_{off} . The linear regime sets in when $t \approx \tau_{\text{off}}$ as is seen from the shorter vertical dashed lines. If we increase the particle concentration, the shape of the curves remains the same but the scattering of curves increases, since $\mathcal{D} \propto 1/\rho^2$ (small k_{off}) and $\mathcal{D} \propto 1 - a\rho$ (large k_{off}).

In Fig. 3, crowder particles diffuse and rebind to a randomly chose site. As we lower k_{off} the separation between τ_{off} and the collision time τ_{coll} increases, which means that the single-file regime ($\langle x^2(t) \rangle \sim \sqrt{t}$) becomes wider. This is simply because crowder particles have not yet started to unbind from the lattice and therefore diffuse collectively in a single-file. We also see that the MSD curves for long times is less scattered than before, indicating that \mathcal{D} is less sensitive to k_{off} . This agrees with our theoretical prediction where $\mathcal{D} \propto \sqrt{k_{\text{off}}}$ compared to $\mathcal{D} \propto k_{\text{off}}$ when crowder particles stand still.

B. Small k_{off} behaviour

In Fig. 4 we show how \mathcal{D} depends on small k_{off} where each panel depicts: (top) immobile crowder particles and rebinding to the same lattice site, (middle), immobile crowder particles and rebinding to a random lattice site, and (bottom) diffusing crowder particles and rebinding to a random site. Symbols represent simulation results and dashed lines the small k_{off} expressions (3)–(5). Each

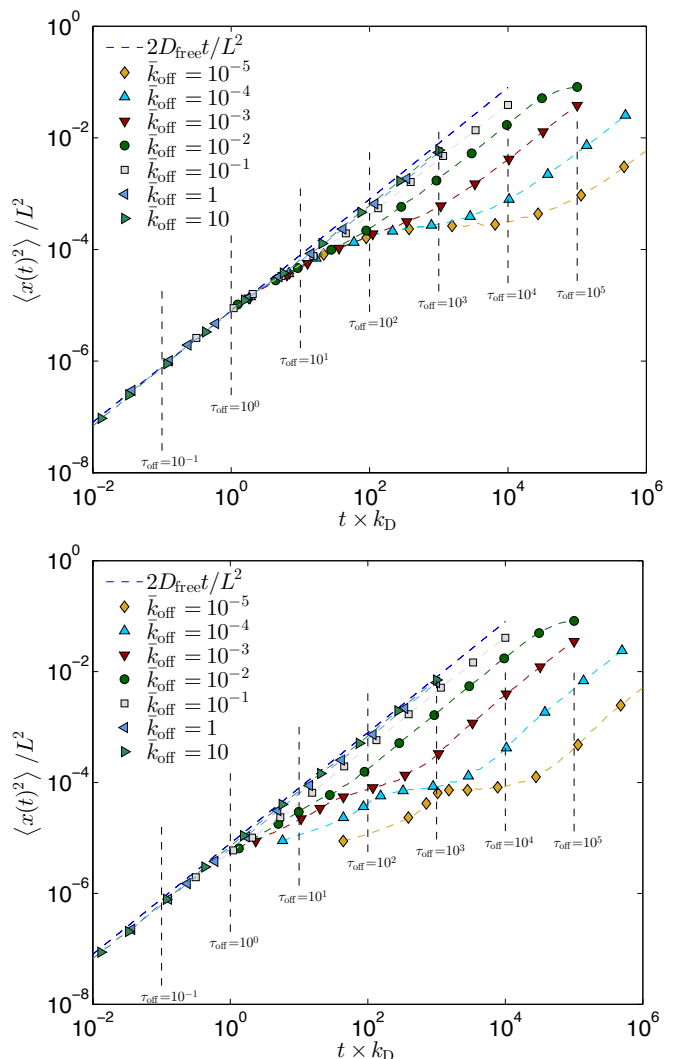


FIG. 2: Mean squared displacement $\langle x^2(t) \rangle$ of the tracer particle as a function of time for different unbinding rates k_{off} when crowder particles do not move. The crowder particles rebind in two ways: to the same site (upper panel), or to a randomly chosen site (lower panel). For shorthand we put $\bar{k}_{\text{off}} = k_{\text{off}}/k_D$ and $\bar{\tau}_{\text{off}} = \tau_{\text{off}}k_D$. Simulation details: lattice constant: $a = 1$, tracer particle diffusion rate: $k_D = 1$ ($k_D = 0$ for crowder particle), filling fraction: $a\rho = 0.1$, number of lattice sites: 501 ($L = 501a$), number of simulation runs: 9600.

case is plotted for two concentrations, $a\rho = 0.1$ and $a\rho = 0.2$. In order to better compare the three panels with the figures below we scaled the vertical axis with the large k_{off} limit $D(1 - a\rho)$. In Fig. 5 we show explicitly how this limit is approached.

The two upper panels in Fig. 4, where the crowder particles are immobile are very similar to each other. If both cases would be depicted in the same graph, the data points would practically sit on top of each other. For clarity, we therefore separated the data into two figures. We see that the small k_{off} behaviour agrees very well with the theoretical results, Eqs. (3) and (4).

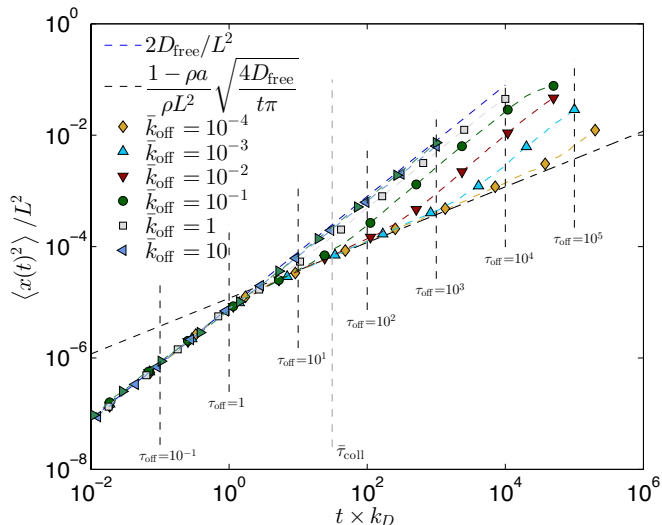


FIG. 3: Mean squared displacement $\langle x^2(t) \rangle$ of the tracer particle as a function of time for different unbinding rates k_{off} when crowder particles diffuse. Rebinding occurs to a randomly chosen site. For shorthand we put $\bar{k}_{\text{off}} = k_{\text{off}}/k_D$, $\bar{\tau}_{\text{off}} = \tau_{\text{off}}k_D$, and $\bar{\tau}_{\text{coll}} = \tau_{\text{coll}}k_D$. Simulation details: lattice constant: $a = 1$, diffusion rate: $k_D = 1$ (for all particles including the tracer), filling fraction: $a\rho = 0.1$, number of lattice sites: 501 ($L = 501a$), number of simulation runs: 9600.

The lower panel depicts when crowder particles diffuse on the lattice. Their movements lead to an overall increase of \mathcal{D} for the tracer particle since they no longer act as static road blocks. This also changes the scaling with k_{off} from linear in the two upper panels, to $\sqrt{k_{\text{off}}}$. The density dependence is also weaker ($1/\rho$ compared to $1/\rho^2$).

C. Large k_{off} behaviour

When k_{off} is much larger than the diffusion rate k_D , we expect the mean field result Eq. (6) to hold. We also expect that corrections to this result becomes increasingly prominent as k_{off} is lowered. Both are confirmed by simulations in Fig. 5, where we see that $\mathcal{D}/(1 - a\rho) \approx 1$ for $k_{\text{off}}/k_D \gtrsim 1$, and $\mathcal{D}/(1 - a\rho) < 1$ for $k_{\text{off}}/k_D < 1$. These results validate the mean field argument leading up to Eq. (6) for our quasi one dimensional system. The figure only shows the case where the crowder particles rebound to the same location, since the behaviour at large k_{off} is close to identical for all rebinding modes.

D. Interpolation formula

In Sec III we proposed Eq. (7) that ties together the small and large k_{off} regimes. The comparison to the full range of k_{off} is shown in Fig. 6 as solid lines (symbols are simulation results). Just as in Fig. 4, each panel shows:

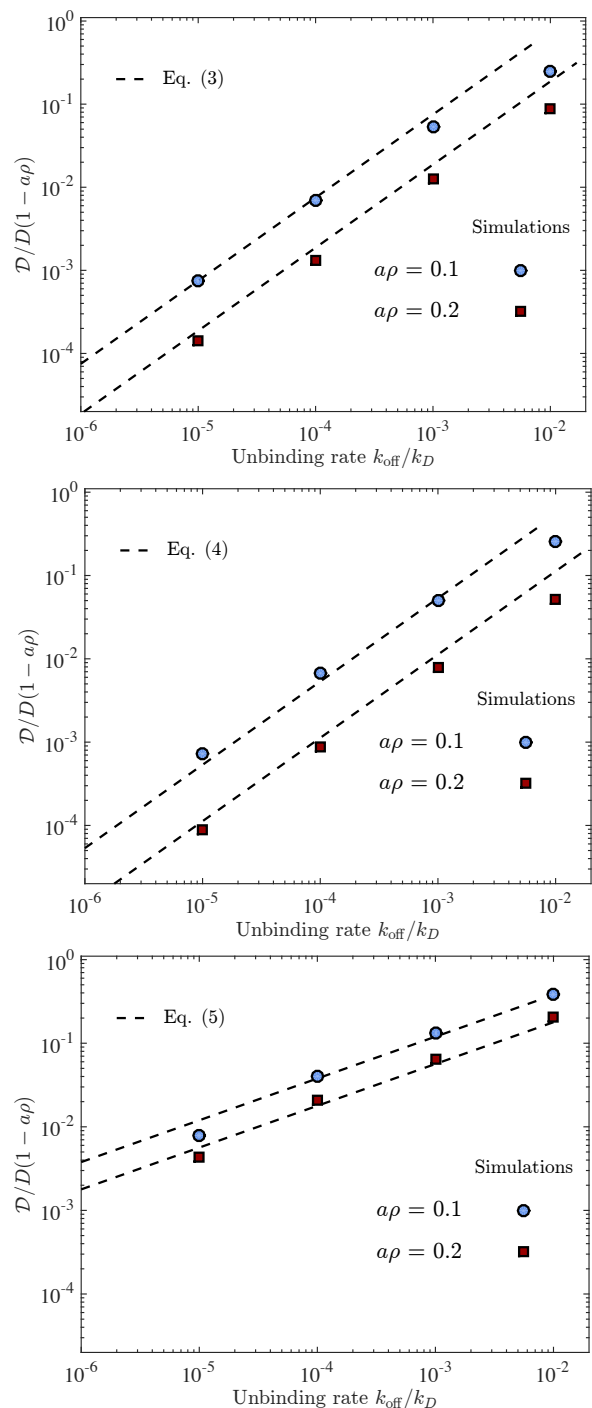


FIG. 4: Long time diffusion constant \mathcal{D} as a function of the unbinding rate k_{off} , when k_{off} is small. Symbols represent simulations for the filling fractions $a\rho = 0.1$ and $a\rho = 0.2$. The dashed lines show our predictions Eqs. (3)–(5). Each panel depicts: (top) immobile crowder particles with rebinding to the same location (middle) immobile crowder particles with rebinding to a random location, (bottom) diffusing crowder particles with rebinding to a random location. The data points are extracted from linear fits of Figs. 2–3 (see Appendix B). R^2 -values from those fits are larger than 0.98.

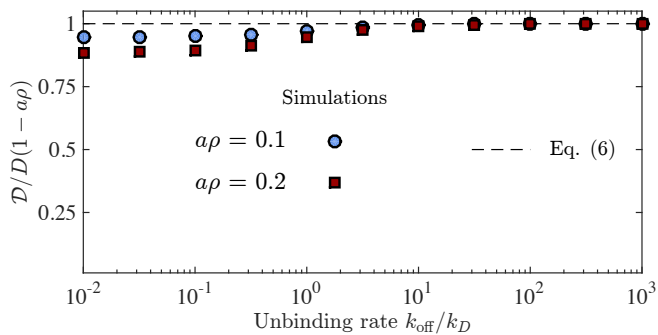


FIG. 5: Long time diffusion constant \mathcal{D} as a function of the unbinding rate k_{off} , when k_{off} is large. Simulation details are the same as in Figs. 2 and 4.

(top) immobile crowder particles and rebinding to the same lattice site, (middle), immobile crowder particles and rebinding to a random lattice site, and (bottom) diffusing crowder particles and rebinding to a random site. Overall, Eq. (7) is a good approximation for the whole range of k_{off} . The deviations are largest in the transition region, roughly $10^{-3} < k_{\text{off}}/k_D < 10^{-1}$, where the maximum relative error for all curves is 79% (top panel, $a\rho = 0.2$). The relative error in the small and large k_{off} tails is less than 7%.

V. SUMMARY AND CONCLUDING REMARKS

We studied the long-time diffusion constant \mathcal{D} of a tracer particle in a one dimensional crowded many-particle system. We found that \mathcal{D} depends strongly on the unbinding rate k_{off} of the surrounding crowder particles and density ρ . For small k_{off} we made a simple theoretical model where we deduced that $\mathcal{D} \sim k_{\text{off}}/\rho^2$ (to first order in $1/\rho^2$) when crowder particles are immobile and only unbind/rebind to the lattice. The prefactor depends on how they rebind, either to the same or to a random site. When they also diffuse we obtain $\mathcal{D} \sim \sqrt{Dk_{\text{off}}}/\rho^2$ (to first order in $1/\rho$), a different k_{off} -scaling than before; D is the free particle diffusion constant. This means that \mathcal{D} is less sensitive to k_{off} and ρ when crowder particles are diffusing compared to standing still. For large k_{off} , we found that all cases agreed with the mean field result $\mathcal{D} \simeq D(1 - \rho a)$, independent of k_{off} . Our new expressions showed overall good agreement with simulations.

It is interesting to see which k_{off}/k_D regime we expect to find in the living cell. As mentioned in the introduction, residence times of DNA binding proteins vary from fractions of a second to up to an hour (unspecific binding is even shorter, >5 ms [39]). To get an order of magnitude estimate of k_{off}/k_D , let us assume that $k_{\text{off}} \sim 0.1 \text{ s}^{-1}$ which lies between the *in vivo* values for the LexA and Gal4 transcription factors. One dimensional diffusion constants also have a big variation. They are in the range $D_{1D} \sim 10^5 - 10^7 \text{ (bp)}^2 \text{ s}^{-1}$ ($\approx 0.01 - 0.1 \mu\text{m}^2 \text{ s}^{-1}$)

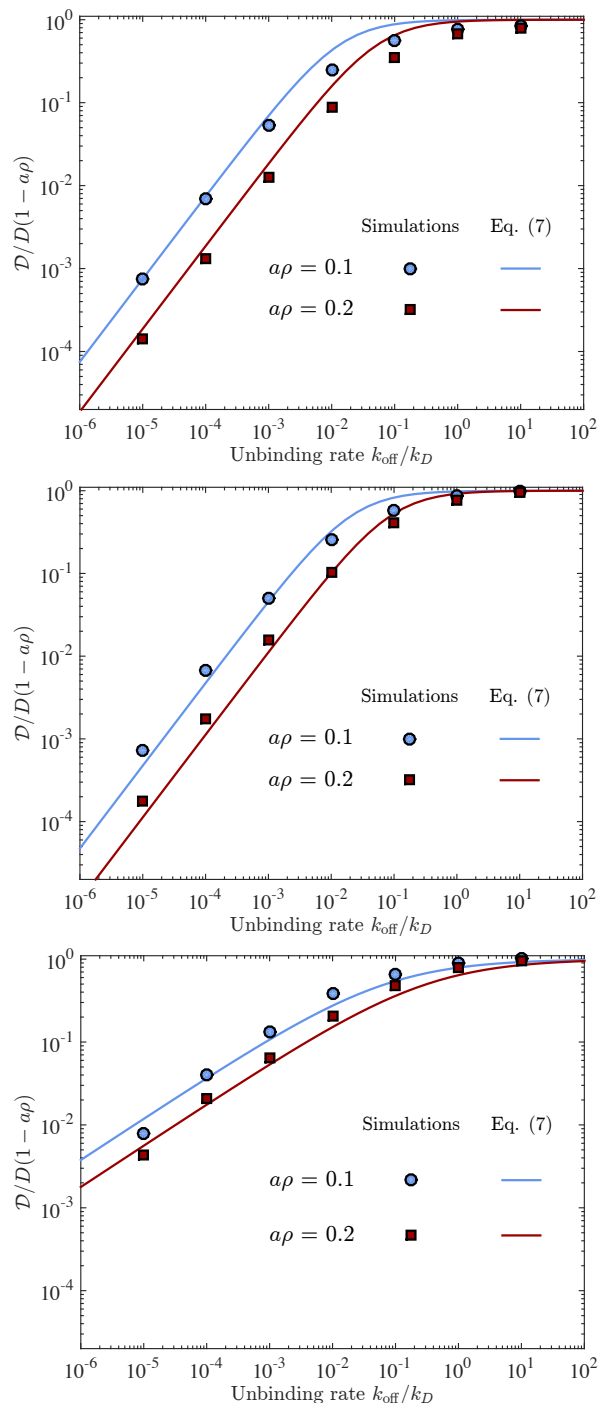


FIG. 6: Long time diffusion constant \mathcal{D} as a function of the unbinding rate k_{off} . Symbols represent simulations for two different filling fractions, $a\rho = 0.1$ and $a\rho = 0.2$. The solid lines show the interpolation formula Eq. (7). Each panel depicts: (top) immobile crowder particles with rebinding to the same location, (middle) immobile crowder particles with rebinding to a random location, (bottom) diffusing crowder particles with rebinding to a random location. The data points are a compilation from Figs. 4 and 5.

[26], which gives $k_D = D_{1D}/(\text{bp})^2 \sim 10^5 - 10^7 \text{ s}^{-1}$. This means that $k_{\text{off}}/k_D \sim 10^{-6} - 10^{-8}$, which clearly indicates that $k_{\text{off}} \ll k_D$.

The model we studied is inspired by protein diffusion on DNA. Our results are simple formulas for the diffusion constant of a tracer particle taking crowding and binding/unbinding dynamics into account. Although a protein is more complex than a hard-core particle, we hope that the simplicity of our results will find its usefulness in a range of settings, in particular, single-molecule tracking experiments.

VI. ACKNOWLEDGEMENTS

LL acknowledges the Knut and Alice Wallenberg foundation and the Swedish Research Council (VR), grant no. 2012-4526, for financial support. TA is grateful to VR for funding (grant no. 2009-2924).

Appendix A: Simple model for \mathcal{D} when k_{off} is small

In this appendix we outline the derivation for the long time diffusion constant \mathcal{D} in the small k_{off} limit that led to Eqs. (3)–(5). The main idea is to calculate the typical length scale l_0 that the tracer travels before being hindered by a crowder particle. In terms of l_0 , the long time diffusion constant is

$$\mathcal{D} = \frac{l_0^2}{2\tau}, \quad (\text{A1})$$

where τ is the typical waiting time until a successful jumping event. Since the diffusion rate k_D is fast, the rate limiting step for the tracer particle to move is when a flanking crowder particle unbind from the lattice. We can therefore envision the tracer particle diffusion as a single particle diffusion process on a coarse grained lattice, with lattice constant l_0 and jump rate $1/\tau$.

First we address τ , the average time until a successful jumping event. Imagine that the tracer particle is flanked by two crowder particles, and the time for any of them to unbind is $1/2k_{\text{off}}$. Now, say that the tracer's right neighbour unbinds but the tracer anyway tries to jump left. This jump is forbidden, and so is in fact half of all tries the tracer makes. This implies that τ is $1/k_{\text{off}}$ rather than $1/2k_{\text{off}}$. Moreover, we also consider rebinding of crowder particles, so even if the tracer move in the direction of the unbound neighbour it may anyway be blocked by another crowder particle. We must therefore correct the jumprate with the probability that the site is vacant, that is $1 - a\rho$ (in equilibrium). In summary, we estimate τ as

$$\tau = \frac{1}{k_{\text{off}}(1 - a\rho)} \quad (\text{A2})$$

Second we turn our attention to the coarse-grained lattice distance l_0 . In short, we choose l_0 the standard deviation of the distribution of nearest-neighbour distances.

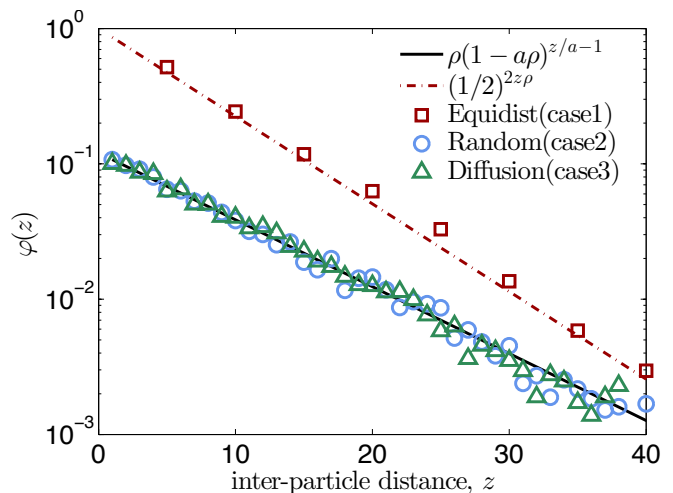


FIG. 7: Distribution of distances between nearest neighbours $\varphi(z)$ in semi-log scale. Symbols depict simulation results, and dashed curves are theoretical results. The filling fraction is $a\rho = 0.1$. The remaining simulation details are the same as in Figs. 2 and 3.

Here is how we formally arrive at this result. Since it can happen that nearest and next-to-nearest neighbours are unbound simultaneously, the length that the tracer particle can move, z , can vary. We choose the probability distribution of z to be the probability that there is a separation z between two nearest neighbour particles. The distribution of z , $\varphi(z)$, is known (see Fig. 7), but differs depending on the type of rebinding. If z only can change in discrete steps of Δ , that is $\Delta, 2\Delta, 3\Delta, \dots$, we can define a jump length distribution $g(l)$ for the tracer particle in the coarse grained lattice as

$$g(l) = \sum_{n=-\infty}^{\infty} \delta(l + n\Delta)\varphi(n\Delta), \quad (\text{A3})$$

where $\delta(x)$ is the Dirac delta function. Now we choose l_0 as the standard deviation of $g(l)$, and from Eq. (A3) one can show that

$$l_0 = \Delta\sqrt{\langle n^2 \rangle_{\varphi}} \quad (\text{A4})$$

where $\langle n^2 \rangle_{\varphi} = \sum_{n=1}^{\infty} n^2\varphi(n\Delta)$. In the subsections below, we calculate l_0 explicitly for the special cases: (1) immobile crowder particles placed equidistantly, (2) immobile crowder particles placed at a random distance apart from each other, and (3) diffusing crowder particles.

1. Case 1: Immobile crowder particles placed equidistantly

In the simulations, the crowder particles sit equidistantly, and unbind and rebind with rates k_{off} and k_{on} , respectively. In order to make sure that the average density ρ is constant over time, we choose $k_{\text{on}} = k_{\text{off}}$, and

work with $2m$ particles in the whole system (lattice + surrounding bulk). This means that m particles will on average be on the lattice and the density is $\rho = m/(aN)$, where N is the number of lattice sites, and a the lattice constant. The smallest separation between two crowder particles in this setup becomes $\Delta = 1/(2\rho)$, and increase discrete steps of Δ :

$$\frac{1}{2\rho}, \frac{1}{\rho}, \frac{3}{2\rho}, \dots \quad (\text{A5})$$

Each one of these lengths has a different probability, and the distribution of nearest neighbour distances is

$$\varphi\left(\frac{n}{2\rho}\right) = \begin{cases} \frac{1}{2} \left(\frac{1}{2}\right)^{|n|}, & n = \pm 1, \pm 2, \dots \\ 0, & n = 0, \end{cases} \quad (\text{A6})$$

which agrees well with simulations (Fig. 7). Using that $\langle n^2 \rangle_\varphi = 6$ in Eq. (A4) gives

$$l_0 = \frac{1}{\rho} \sqrt{\frac{3}{2}}. \quad (\text{A7})$$

2. Case 2: Immobile crowder particles with rebinding to random locations

In this case the crowder particles leave the lattice and return to a random vacant lattice site. This means that the smallest separation is the lattice distance of the original lattice, $\Delta = a$, and distances are in steps of a :

$$a, 2a, 3a, \dots \quad (\text{A8})$$

The inter-particle distance distribution in this case is

$$\varphi(na) = \begin{cases} \frac{1}{2} \frac{a\rho}{1-a\rho} (1-a\rho)^{|n|}, & n = \pm 1, \pm 2, \dots \\ 0, & n = 0 \end{cases} \quad (\text{A9})$$

which is corroborated by simulations in Fig. 7. In the continuum limit (small a), the distribution becomes exponential $\varphi(na) \sim e^{-|n|a\rho}$. Using that $\langle n^2 \rangle_\varphi = (2 - a\rho)/(2a^2\rho^2)$, we obtain

$$l_0 = \frac{1}{\rho} \sqrt{\frac{2 - a\rho}{2}}. \quad (\text{A10})$$

3. Case 3: Diffusing crowder particles with rebinding to random locations

Here all particles diffuse which drastically changes the situation. The main difference is that the tracer does not get stuck between two flanking road blocks since they also move. However, we know from simulations that the MSD for the tracer is in the long time limit proportional to Dt (Fig. 3), which is a direct manifestation that the no-passing condition is violated (otherwise we would have had $\text{MSD} \sim \sqrt{t}$). Altogether, this implies that there is

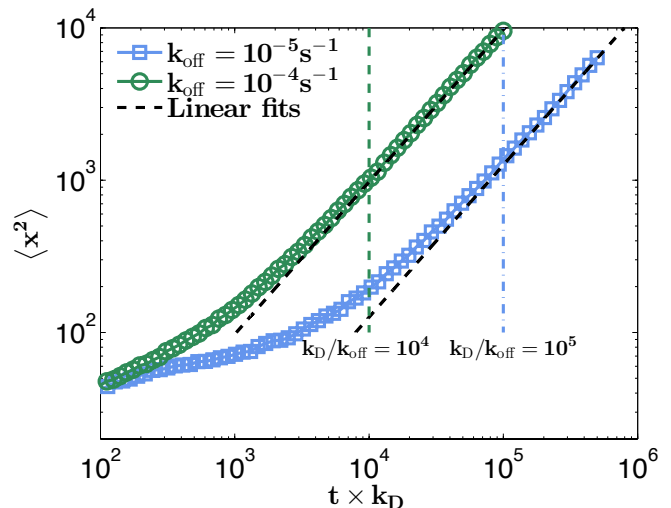


FIG. 8: MSD of the tracer particle as a function of time for two different unbinding rates. The dashed black lines are linear fits of the MSD curves for times $t \geq \tau_{\text{off}}$. The simulation details are the same as in Fig. 2.

length scale for the coarse grained lattice and a time scale associated with a jumping event.

For this case we cannot use $\varphi(z)$ to estimate l_0 since $\varphi(z)$ is the same as when crowder particles are immobile (see Fig. 7, \circ and \triangle), and gives the wrong result for \mathcal{D} . The reason is that inter-particle distances fluctuate at the same rate as the tracer is diffusing, and those fluctuations increase \mathcal{D} . In fact, even if $k_{\text{off}} = 0$, the tracer particles still can move across the system, although slowly. We estimate l_0 as the distance the tracer particle explores in a time τ , that is

$$l_0 = \sqrt{\langle x^2(t = \tau) \rangle} = \left(\frac{4D}{\pi k_{\text{off}}} \frac{1 - a\rho}{\rho^2} \right)^{1/4} \quad (\text{A11})$$

Interestingly, l_0 depends on k_{off} and not only ρ as in the previous cases. This changes the scaling of k_{off} in \mathcal{D} from linear in Cases 1 and 2 to $\sqrt{k_{\text{off}}}$ for this case. This can also be understood from the following simple argument. The curve for $\langle x^2(t) \rangle$ is continuous for all times, and at some time the dynamics changes behaviour from single-file ($\sim \sqrt{t}$) to regular diffusion ($\sim t$). This occurs around $t \approx \tau$, which implies

$$2Dt \Big|_{t=\tau} \approx \sqrt{\frac{4Dt}{\pi\rho^2}} \Big|_{t=\tau}. \quad (\text{A12})$$

This yields $\mathcal{D} \propto \sqrt{k_{\text{off}}}$.

Appendix B: Extraction of the long time diffusion constant

The way we determine \mathcal{D} from our MSD simulations, is illustrated in Fig. 8. First, τ_{off} is the approximate

time at which the MSD becomes linear (shown as vertical dashed-dotted lines). Second, we make a linear regression of the MSD curve starting from that point, and obtain the slope which equals $2D$. The resulting fits are shown as dashed lines.

Appendix C: Numerical implementation

The model (Fig. 1) is implemented using the Gillespie algorithm [40]. The majority of the details of the implementation has been explained elsewhere [34], but below we point out some key differences.

We keep track of the unbound crowder particles in the bulk in order to have the option to rebind them at the location they detached from. In practice we use two

lattices, one of which represents the bulk. The filling fraction is maintained at the level we want by setting $k_{\text{on}} = k_{\text{off}}$, and then let the systems equilibrate such that half the number of crowder particles sit in the bulk and the other half on the lattice we are interested in. This representation helpful to investigate all sorts of binding modes especially rebinding to the same location. In Ref. [34] the bulk served as an infinite particle reservoir and the concentration on the lattice was tuned via detailed balance (rebinding always occurred to a randomly chosen site). Here on the other hand, the bulk has a finite size and cannot be seen as a strict particle reservoir. However, since we use about 500 particles, fluctuations around the filling fraction $a\rho$ are so small that we rarely (if ever) deplete the bulk. This means that we have approximately a grand canonical ensemble.

-
- [1] Huan-Xiang Zhou, Germán Rivas, and Allen P Minton. Macromolecular crowding and confinement: biochemical, biophysical, and potential physiological consequences. *Annual review of biophysics*, 37:375, 2008.
- [2] Steven B Zimmerman and Stefan O Trach. Estimation of macromolecule concentrations and excluded volume effects for the cytoplasm of *escherichia coli*. *Journal of molecular biology*, 222(3):599–620, 1991.
- [3] R John Ellis. Macromolecular crowding: obvious but underappreciated. *Trends in biochemical sciences*, 26(10):597–604, 2001.
- [4] G W Li, O G Berg, and J Elf. Effects of macromolecular crowding and dna looping on gene regulation kinetics. *Nature Physics*, 5(4):294–297, 2009.
- [5] Shu-ichi Nakano, Hisae Tateishi Karimata, Yuichi Kitagawa, and Naoki Sugimoto. Facilitation of rna enzyme activity in the molecular crowding media of cosolutes. *Journal of the American Chemical Society*, 131(46):16881–16888, 2009.
- [6] Huan-Xiang Zhou. Protein folding and binding in confined spaces and in crowded solutions. *Journal of Molecular Recognition*, 17(5):368–375, 2004.
- [7] Jörg Martin. Requirement for groel/groes-dependent protein folding under nonpermissive conditions of macromolecular crowding. *Biochemistry*, 41(15):5050–5055, 2002.
- [8] Daniel S Banks and Cécile Fradin. Anomalous diffusion of proteins due to molecular crowding. *Biophysical journal*, 89(5):2960–2971, 2005.
- [9] Felix Höfling and Thomas Franosch. Anomalous transport in the crowded world of biological cells. *Reports on Progress in Physics*, 76(4):046602, 2013.
- [10] T. Knorpp and M.F Templin. Method of the year 2008. *Nature methods*, 6(1):1, 2009.
- [11] Fredrik Persson, Irmeli Barkefors, and Johan Elf. Single molecule methods with applications in living cells. *Current opinion in biotechnology*, 24(4):737–744, 2013.
- [12] Iddo Heller, Gerrit Sitters, Onno D Broekmans, Géraldine Farge, Carolin Menges, Wolfgang Wende, Stefan W Hell, Erwin JG Peterman, and Gijs JL Wuite. Sted nanoscopy combined with optical tweezers reveals protein dynamics on densely covered dna. *Nature methods*, 10(9):910–916, 2013.
- [13] Anders Karlsson, Roger Karlsson, Mattias Karlsson, Ann-Sofie Cans, Anette Strömberg, Frida Ryttsén, and Owe Orwar. Molecular engineering: networks of nanotubes and containers. *Nature*, 409(6817):150–152, 2001.
- [14] Cees Dekker. Solid-state nanopores. *Nature nanotechnology*, 2(4):209–215, 2007.
- [15] Tadashi Ando and Jeffrey Skolnick. Crowding and hydrodynamic interactions likely dominate in vivo macromolecular motion. *Proceedings of the National Academy of Sciences*, 107(43):18457–18462, 2010.
- [16] James A Dix and AS Verkman. Crowding effects on diffusion in solutions and cells. *Annu. Rev. Biophys.*, 37:247–263, 2008.
- [17] Sean R McGuffee and Adrian H Elcock. Diffusion, crowding & protein stability in a dynamic molecular model of the bacterial cytoplasm. *PLoS computational biology*, 6(3):e1000694, 2010.
- [18] Paulo A Netz and Thomas Dorfmueller. Computer simulation studies of diffusion in gels: Model structures. *The Journal of chemical physics*, 107(21):9221–9233, 1997.
- [19] Matthias Weiss, Markus Elsner, Fredrik Kartberg, and Tommy Nilsson. Anomalous subdiffusion is a measure for cytoplasmic crowding in living cells. *Biophysical journal*, 87(5):3518–3524, 2004.
- [20] Surya Ghosh, Andrey G Cherstvy, and Ralf Metzler. Non-universal tracer diffusion in crowded media of non-inert obstacles. *Physical Chemistry Chemical Physics*, 2014.
- [21] Michael J Saxton. Anomalous diffusion due to binding: a monte carlo study. *Biophysical journal*, 70(3):1250–1262, 1996.
- [22] Jędrzej Szymanski and Matthias Weiss. Elucidating the origin of anomalous diffusion in crowded fluids. *Physical review letters*, 103(3):038102, 2009.
- [23] A Marcovitz and Y Levy. Obstacles may facilitate and direct dna search by proteins. *Biophysical journal*, 104(9):2042–2050, 2013.
- [24] Won-Ki Cho, Cherlhyun Jeong, Daehyung Kim, Minhyeok Chang, Kyung-Mi Song, Jeungphil Hanne, Changill Ban, Richard Fishel, and Jong-Bong Lee. Atp alters the diffusion mechanics of muts on mismatched

- dna. *Structure*, 20(7):1264–1274, 2012.
- [25] Yi Luo, Justin A North, Sean D Rose, and Michael G Poirier. Nucleosomes accelerate transcription factor dissociation. *Nucleic acids research*, 42(5):3017–3027, 2014.
- [26] Jason Gorman and Eric C Greene. Visualizing one-dimensional diffusion of proteins along dna. *Nature structural & molecular biology*, 15(8):768–774, 2008.
- [27] T E Harris. Diffusion with” collisions” between particles. *Journal of Applied Probability*, 2(2):323–338, 1965.
- [28] D G Levitt. Dynamics of a single-file pore: non-fickian behavior. *Physical Review A*, 8(6):3050, 1973.
- [29] J K Percus. Anomalous self-diffusion for one-dimensional hard cores. *Physical Review A*, 9(1):557, 1974.
- [30] M Kollmann. Single-file diffusion of atomic and colloidal systems: Asymptotic laws. *Physical Review Letters*, 90(18):180602, 2003.
- [31] L Lizana and T Ambjörnsson. Single-file diffusion in a box. *Physical Review Letters*, 100(20):200601, 2008.
- [32] E Barkai and R Silbey. Theory of single file diffusion in a force field. *Physical Review Letters*, 102(5):50602, 2009.
- [33] M A Lomholt, L Lizana, and T Ambjörnsson. Dissimilar bouncy walkers. *Journal of Chemical Physics*, 134(4):045101, 2011.
- [34] Robin Forsling, Lloyd P Sanders, Tobias Ambjörnsson, and Ludvig Lizana. Non-markovian effects in the first-passage dynamics of obstructed tracer particle diffusion in one-dimensional systems. *The Journal of chemical physics*, 141(9):094902, 2014.
- [35] A B Kolomeisky. Physics of protein–dna interactions: mechanisms of facilitated target search. *Physical Chemistry Chemical Physics*, 13(6):2088–2095, 2011.
- [36] O Bénichou, C Loverdo, M Moreau, and R Voituriez. Intermittent search strategies. *Reviews of Modern Physics*, 83(1):81, 2011.
- [37] Joseph W Haus and Klaus W Kehr. Diffusion in regular and disordered lattices. *Physics Reports*, 150(5):263–406, 1987.
- [38] Kazuo Nakazato and Kazuo Kitahara. Site blocking effect in tracer diffusion on a lattice. *Progress of Theoretical Physics*, 64(6):2261–2264, 1980.
- [39] Johan Elf, Gene-Wei Li, and X Sunney Xie. Probing transcription factor dynamics at the single-molecule level in a living cell. *Science*, 316(5828):1191–1194, 2007.
- [40] D T Gillespie. A general method for numerically simulating the stochastic time evolution of coupled chemical reactions. *Journal of Computational Physics*, 22(4):403–434, 1976.